Electronic Supplementary Material (ESI) for Chemical Science

Novel Lanthanide Nanoparticle Frameworks for Highly-Efficient Photoluminescence and Hypersensitive Detection

Yuan-Jun Tong,[a] Lu-Dan Yu,[a] Nan Li,[a] Minhui Shen,[a] Xiaoru Peng,[a] Huangsheng Yang,[a] Yu-Xin Ye,[a] Fang Zhu,[a] Janusz Pawliszyn,[b] Jianqiao Xu,[a,*] Gangfeng Ouyang[a,c,d,*]

a MOE Key Laboratory of Bioinorganic and Synthetic Chemistry/KLGHEI of Environment and Energy Chemistry, School of Chemistry, Sun Yat-sen University, Guangzhou, Guangdong 510006 (P. R. China)

E-mail: xujq27@mail.sysu.edu.cn (J. Xu); cesoygf@mail.sysu.edu.cn (G. Ouyang)

b Department of Chemistry, University of Waterloo, Waterloo, Ontario N2L3G1 (Canada).

c Chemistry College, Center of Advanced Analysis and Gene Sequencing, Zhengzhou University, Kexue Avenue 100, Zhengzhou 450001 (P. R. China)

d Guangdong Provincial Key Laboratory of Emergency Test for Dangerous Chemicals, Guangdong Institute of Analysis (China National Analytical Center Guangzhou), Guangdong Academy of Sciences, 100 Xianlie Middle Road, Guangzhou 510070 (P. R. China)

1. EXPERIMENTAL SECTION

1.1 Apparatus.

All reagents of analytical grades were obtained from commercial sources and used without further purification. The UV-vis absorption spectra were collected on an UV-2450 spectrophotometer (Shimadzu, Japan). JEOL2010 transmission electron microscope (TEM, Japan) were used to characterize the morphologies of the materials. Fluorescence spectra were performed on an F-97 Pro fluorescence spectrometer (Shanghai Lingguang Technology Co. LTD, Shanghai, China). The slit widths (including excitation and emission) and the photomultiplier tube (PMT) voltage were set at 10 nm and 750 V, respectively. The X-ray photoelectron spectroscopy (XPS) was conducted with a Thermo ESCALAB 250 spectrometer (USA) using an Al Ka monochromator source (*hv*=1486.6 eV) and a multidetection analyzer. Fourier transform infrared (FTIR) spectra were recorded in the 4000-400 cm^{-1} region using KBr pellets and a Nicolet/Nexus-670 FTIR spectrometer. Powder X-ray diffraction patterns (PXRD) were determined with a Rigaku Smart Lab diffractometer (Bragg-Brentano geometry, Cu Kα1 radiation, λ = 1.54056 Å).

1.2 Synthesis of COF1.

A Necked quartz tube was charged with 2,5-divinylterephthalaldehyde (DVA, 55.9 mg, 0.3 mmol) and 1,3,5-tri(4-aminophenyl)benzene (TAPB, 70.3 mg, 0.2 mmol). A mixture of 1 mL of o-dichlorobenzene, 1 mL of nBuOH and 0.2 mL of 6 M acetic acid (5:5:1 v/v/v) were subsequently added. After three freeze-pump-thaw cycles, the tube was sealed and stored at room temperature for 15 days. The precipitate was isolated by filtration and washed with THF using Soxhlet extraction for 24 h to ensure the removal of unreacted raw materials and residual oligomers. The product was obtained after dried in vacuum at 80 °C (101 mg, 80%).

1.3 Synthesis of COF1-Heck.

First, 60 mg of COF1 was dissolved in 100 mL of N-Methylpyrrolidone then treated for 30 minutes with a ultrasonic cell disruptor to obtain highly dispersed COF1. Subsequentlly, a mixture of parabromobenzoic acid (50 mg), $Pd(OAc)_2$ (2 mg), N,N-dimethyl-β-alanine hydrocloride (1 mg), K_2CO_3 (126.17 mg) was added into the COF1 suspension and stirred under Ar at 130 °C for 10 h. After the mixture was washed by water, and washed with diethyl ether using Soxhlet extraction for 24 h to ensure the removal of unreacted raw materials, the product was obtained after dried in vacuum at 80 °C. Herein, the post-modification strategy was adopted since the residual modification reagants could be readily removed via washing with proper solvents. By contrast, relatively tedious purification is needed to separate the residual reactants and the product, if the pre-modification strategy is used. In addition, it was estimated that the grafting yield reached 79.5%, which indicated that almost five sides of each hexagon in COF1 were successfully anchoring with carboxyl groups. This high grafting yield was thought capable of stabilizing the clusters in the nanochannels.

1.4 Synthesis of TbNPs@COF1-Heck.

First, COF1-Heck (10 mg) was added into 20 mL of MeOH/MeCN (1:1 v/v) and then treated for 30 minutes by an ultrasonic cell disruptor to obtain highly dispersed COF1-Heck. After that, the MeOH solution of $Tb(NO_3)_3{\cdot}6H_2O$ (1 mL, 100 mM) was mixed with the COF1-Heck suspension. Subsequentlly, triethylamine (0.1 mmol) was added under magnetic strring, followed by the addition of the MeCN solution of 6-chloro-2-pyridinol (CHP, 1 ml, 100 mM) drop by drop. The mixed solution was stirred, while the reaction flask kept open to ensure the volatilization of solvent for 5 day. Then, the TbNPs@COF1-Heck powders were obtained by evaporating the solvent. The powders were washed with methanol, and finally dried.

1.5 Synthesis of pure TbCs.

The pure TbCs was synthesized by referring to the previous work with slight modification.[1, 2] 1.0 mmol of $Tb(NO_3)_3 \cdot 6H_2O$ (0.453 mg) and 1.0 mmol of 6-chloro-2-pyridinol (CHP) (0.130 g) were added in 20 mL of MeOH/MeCN (1:1), followed by the addition of triethylamine (0.139 mL, 1.0 mmol). After 12 hours, the resulting solution was filtered and left undisturbed in an open vial for solvent evaporation under room temperature. Colorless block-like single crystals were obtained in the next 5 days. The powder TbCs was obtained by evaporating the solvent of MeOH/MeCN and then washed with methanol, and finally dried. The molecular formula of the pure TbCs was $[Tb_{20}(chp)_{30}(CO_3)_{12}(NO_3)_6(H_2O)_6]H_2O$.

1.6 Synthesis of COF2 and COF2-Heck.

A Necked quartz tube was charged with 2,5-divinylterephthalaldehyde (55.9 mg, 0.3 mmol) and 1,3,5-Benzenetriamino hydrochloride (46.5 mg, 0.2 mmol). A mixture of 1 mL of o-dichlorobenzene, 1 mL of n-BuOH and 0.2 mL of 6 M acetic acid (5:5:1 v/v/v) were added. After three freeze-pump-thaw cycles, the tube was sealed and heated at 120 °C for 3 days. The precipitate was isolated by filtration and washed with THF using Soxhlet extraction for 24 h to ensure the removal of unreacted raw materials and residual oligomers. The product was obtained after dried in vacuum at 80 °C. Subqsequently, COF2-Heck was prepared by grafting carboxyl groups on the vinyl bonds of COF2. The procedure was the same to section 1.3.

1.7 Synthesis of COF3 and COF3-Heck.

A Necked quartz tube was charged with 2,5-divinylterephthalaldehyde (55.9 mg, 0.3 mmol) and 4,4',4"-(benzene-1,3,5-trityltri(atylene-2,1-diyl))triphenylamine (84.7 mg, 0.2 mmol). A mixture of 1 mL of o-dichlorobenzene, 1 mL of n-BuOH and 0.2 mL of 6 M acetic acid (5:5:1 v/v/v) were added. After three freeze-pump-thaw cycles, the tube was sealed and heated at 120 °C for 3 days. The precipitate was isolated by filtration and

washed with THF using Soxhlet extraction for 24 h to ensure the removal of unreacted raw materials and residual oligomers. The product was obtained after dried in vacuum at 80 °C.

Subqsequently, COF3-Heck was prepared by grafting carboxyl groups on the vinyl bonds of COF3. The procedure was the same to section 1.3.

1.8 EXAFS analysis

Data reduction, data analysis, and EXAFS fitting were performed according to the standard procedures using the ATHENA and ARTEMIS program intergrated within the Demeter packages.[4] For EXAFS modeling, The k_2-weighted EXAFS spectra were obtained via subtracting the post-edge background from the overall absorption, normalization with respect to the edge-jump step, and Fourier transformation to real (R) space using a Hanning windows (dk = 1.0 Å) ranging from 2-10.5 $Å^{-1}$. EXAFS of the sample was fitted in the EXAFS analysis to determine the nominal coordination numbers (CNs) in the Tb-O/Tb-N scattering path in the sample.

1.9 XPS test

In this work, the X-ray photoelectron spectroscopy (XPS) was conducted with a Thermo ESCALAB 250 spectrometer (USA) using an Al Ka monochromator source (*hv*=1486.6 eV) and a multidetection analyzer. The sample was prepared on silicon substrate by aluminum double-tape. The sample based film was loaded into Thermo Fisher Scientific ESCALAB 250 XPS system, where Ar^+ bombardment was performed and surface chemical state of the sample was characterized. XPS spectra were recorded using a monochromated Al Kα (1486.6 eV) X-ray source with the take-off angle of 90° after different Ar^+ bombardment time. The Ar^+ bombardment was operated with EX05 argon ion gun whose angle arrangement given the sample surface normal is 45° at a chamber pressure of $1×10^{-6}$ Pa. The ion beam voltage was 3 kV and the emission current was 2 μA. The spectra were collected and analyzed by

Avantage software.

1.10 Fluorescent spectra collection

Fluorescence spectra (including emission and excitation) were collected on an F-97 Pro fluorescence spectrometer (Shanghai Lingguang Technology Co., LTD, Shanghai). The slit widths and the photomultiplier tube voltage were set at 10 nm and 750 V, respectively. For the collection of the fluorescent spectra of the pure TbCs, 5 mg of the pure TbCs was dispersed into 5 mL of ultrapure water under sonication for 3 min. Subsequently, the stock suspension (50 μL) was diluted with ultrapure water to a fianl volume of 600 μL. The excitation spectra were first collected by detecting the highest characteristic emission of Tb(III) at 545 nm. Subsequentlly, the emission spectra were collected by excited with the highest excitation peak (i.e. 330 nm). The collection of the excitation and emission spectra of TbNPs@COF1-Heck, TbNPs@COF2-Heck, and TbNPs@COF3-Heck were the same to the pure TbCs.

1.11 Fluorescent analysis of UO_2^{2+}.

Firstly, the stock suspension of the pure TbCs was prepared by mixing 5 mg of the pure TbCs to 5 mL of ultrapure water under sonication for 3 min. Subsequently, the TbCs stock suspension (50 μL) and an aliquot of 200 μL sample solution were mixed. The mixture was diluted with ultrapure water to a final volume of 600 μL. The charactistic emission of Tb(III) at 545 nm was measured under the exication of incident light at 330 nm for quantification. The detection of UO_2^{2+} with the other materials (TbNPs@COF1-Heck, TbNPs@COF2-Heck, and TbNPs@COF3-Heck) followed the same procedure.

1.12 Fluorescent analysis of methinehalides.

Firstly, the stock suspension of the pure TbCs was prepared by mixing 5 mg of the pure TbCs to 5 mL of methonal under sonication for 3 min. Subsequently,

the TbCs stock suspension (50 μL) and an aliquot of 200 μL sample solution (in methonal) were mixed. The mixture was diluted with methonal to a final volume of 600 μL. The charactistic emission of Tb(III) at 545 nm was measured under the exication of incident light at 330 nm for quantification. The detection of methonal with the other materials TbNPs@COF2-Heck followed the same procedure.

1.13 Fluorescence quantum yield measurement.

The absolute quantum yields (QY) were calculated as the ratios between the emitted light and the absorbed excitation light by the materials. The measurements were performed using an integrating sphere attached to Edinburgh FLS 1000 with the excitation light at 330 nm from a 450 W Xenon lamp. The suspension of each material was placed in a UV quarts cuvette with a light path of 10 mm to measure its QY. Meanwhile, the solvent (water) filled in another quart's cuvette was used as a blank sample for reference. The spectral correction curve that related to the sensitivity of the monochromator, detector, sphere coating, and optics to wavelength was deducted.

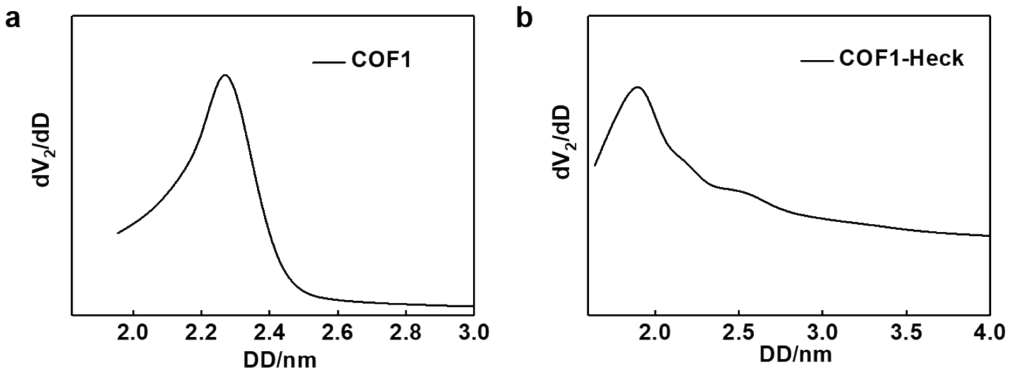

Figure S1. Pore size distribution of (a) COF1 and (b) COF1-Heck, respectively.

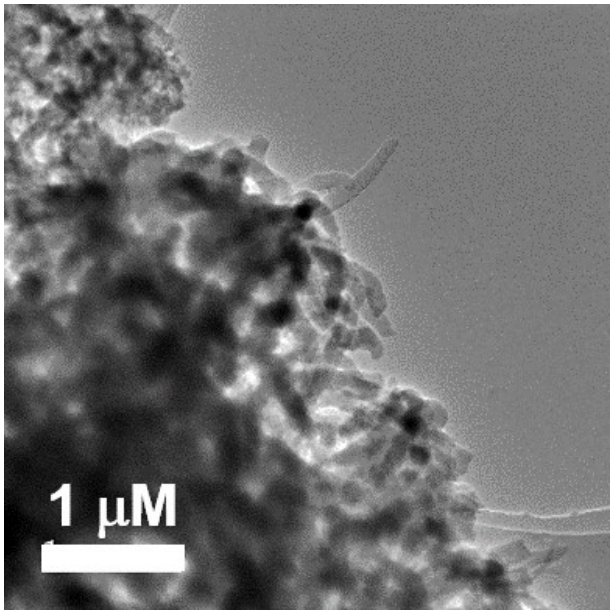

Figure S2. TEM image of COF1.

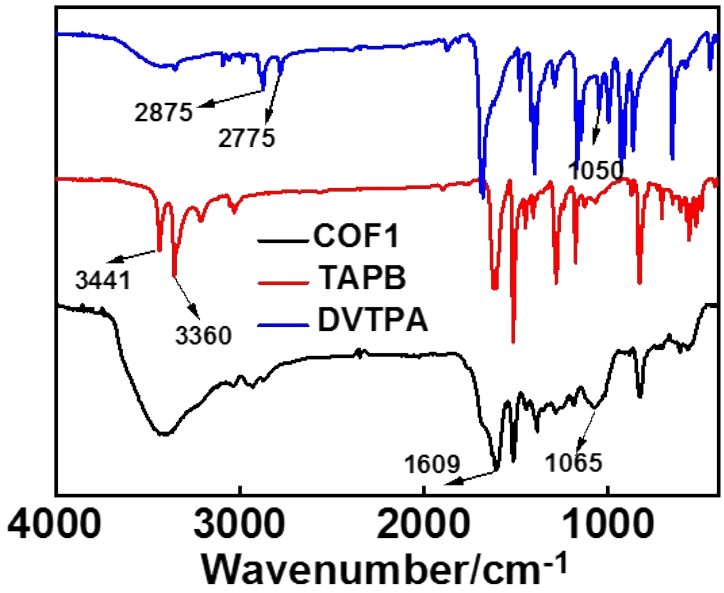

Figure S3. FTIR spectra of COF1, TAPB and DVTPA.

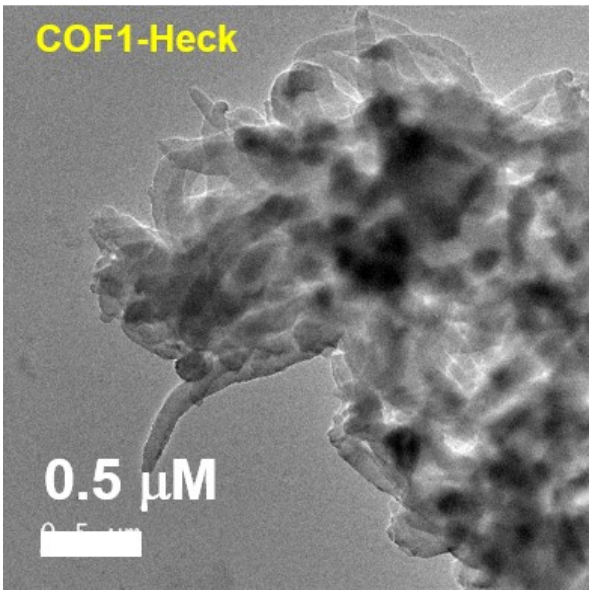

Figure S4. TEM image of COF1-Heck.

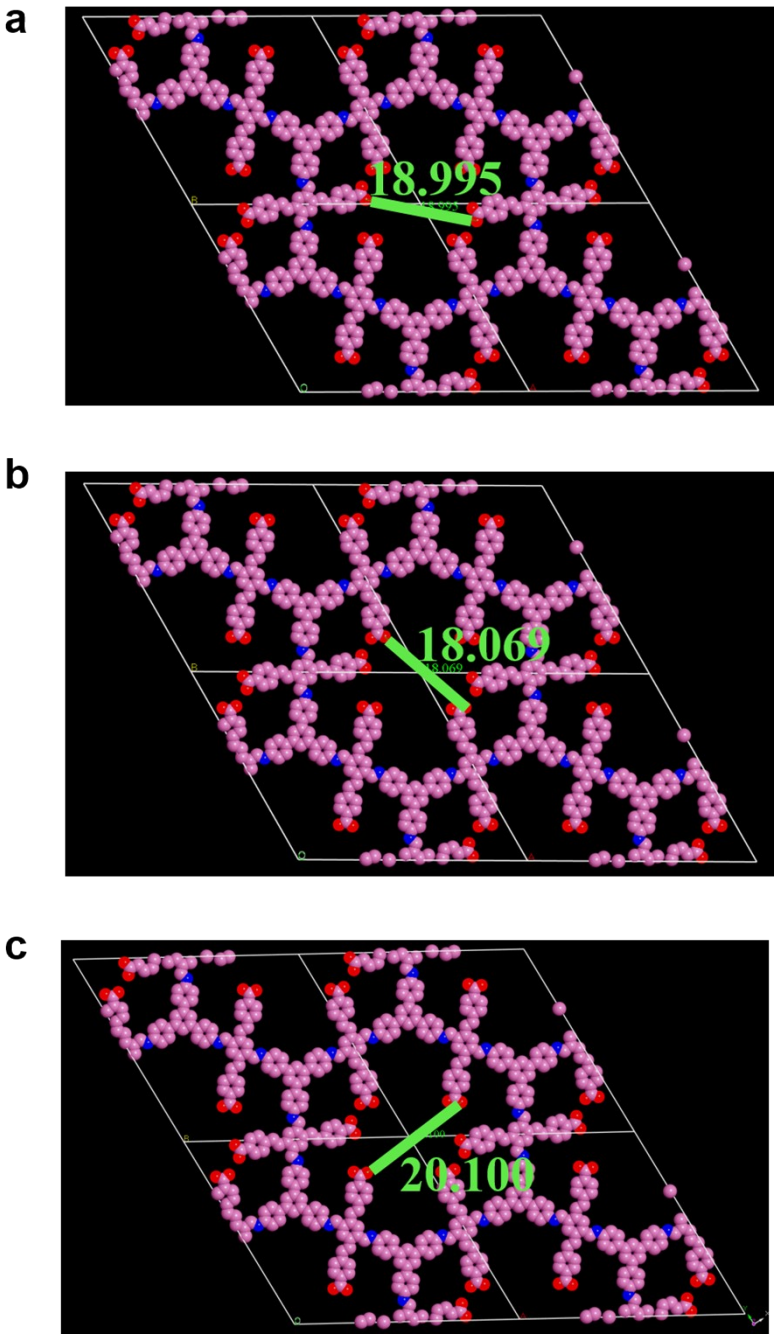

Figure S5. The distances of two opposing carboxyl groups in COF1-Heck, which were stimulated in Materials Studio.

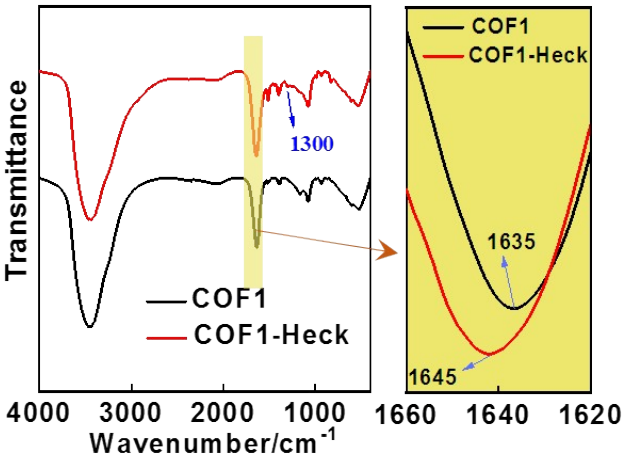

Figure S6. FTIR spectra of of COF1 and COF1-Heck, respectively.

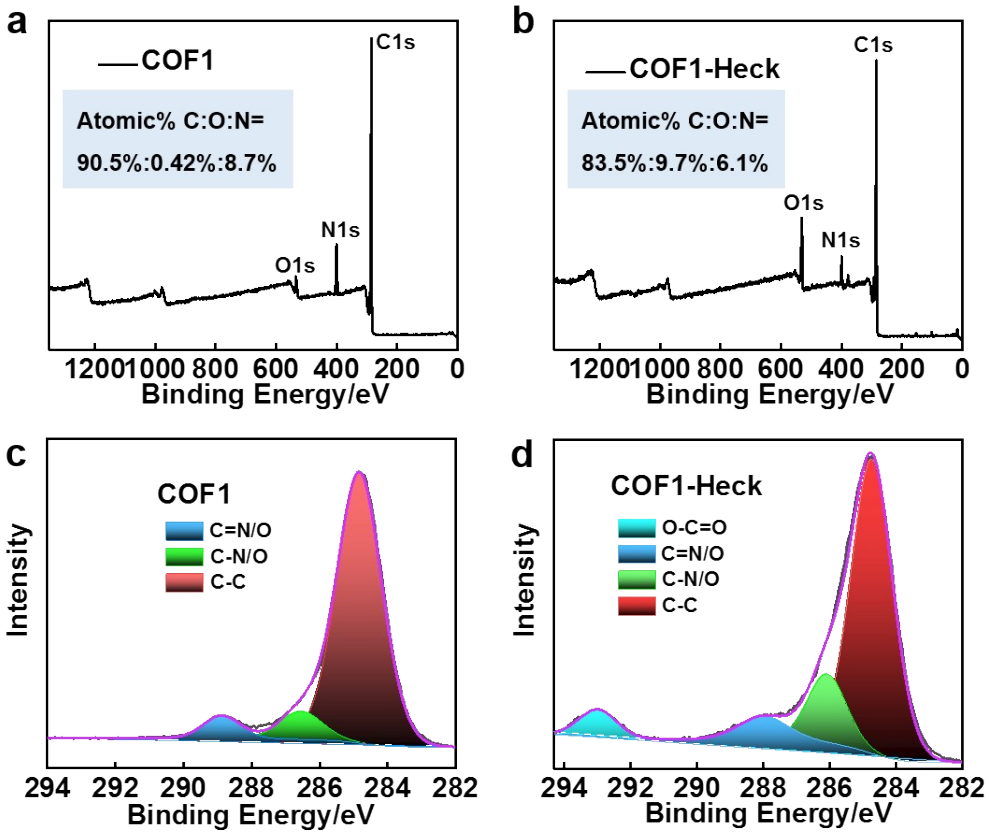

Figure S7. (a) XPS spectrum of COF1. (b) XPS spectrum of COF1-Heck. (c) Refined C1s spectrum of of COF1. (d) Refined C1s spectrum of of COF1-Heck.

Comments: Theoretically, COF1 contains no O element, while the O/N atomic ratio in COF1-Heck should be 2. The experimental atomic ratio of O/N was 1.58 (9.7%/6.1%) in COF1-Heck. And as expected, the O/N atomic ratio can be ignored (0.048, i.e. 0.42%/8.7%) in COF1. Therefore, the grafting yield was calculated to be 79.5% by using the equation below:

$$grafting\ yield = \frac{tested\ ratio\ of\ O/N}{theoritical\ ratio\ of\ O/N} \times 100\%$$

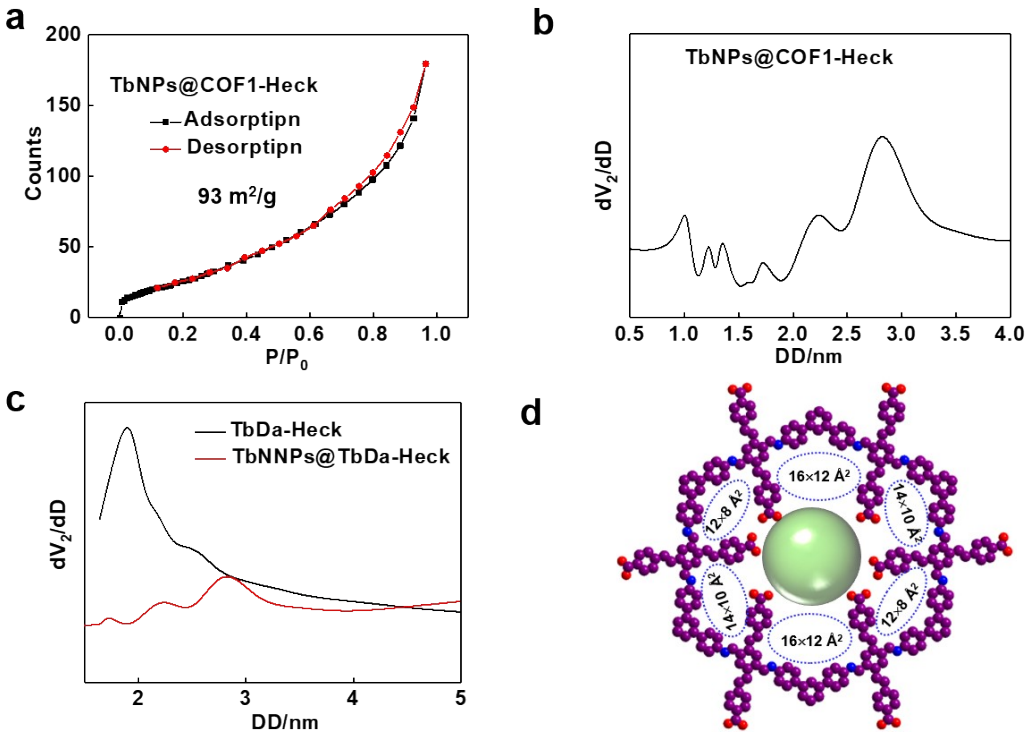

Figure S8. (a) N_2 isothermal adsorption-desorption curve of TbNPs@COF1-Heck. (b) Pore size distribution of TbNPs@COF1-Heck. (c) The overlaid pore size distribution of TbNPs@COF1-Heck and COF1-Heck. (d) Simulated secondary pores of TbNPs@COF1-Heck.

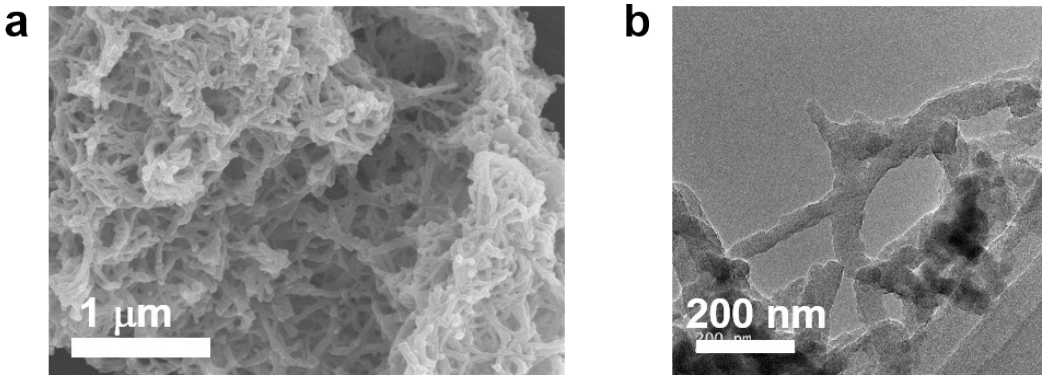

Figure S9. (a) SEM and (b) TEM images of TbNPs@COF1-Heck.

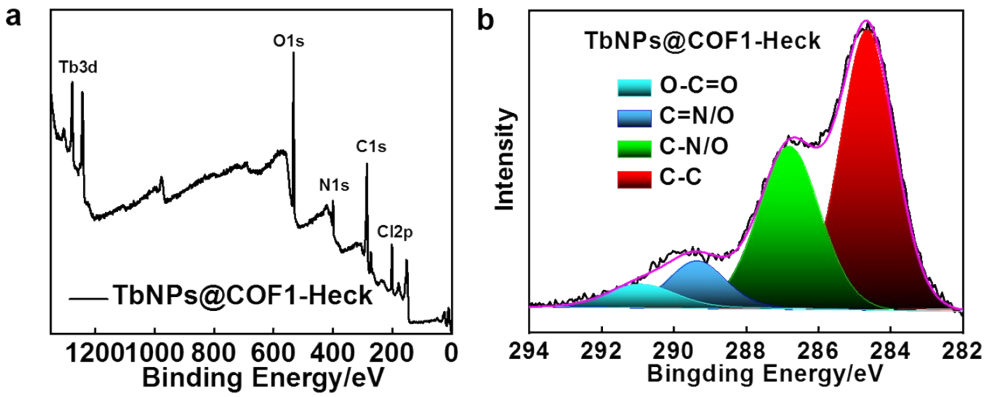

Figure S10. (a) XPS spectrum of TbNPs@COF1-Heck. (b) Refined C1s spectrum of TbNPs@COF1-Heck.

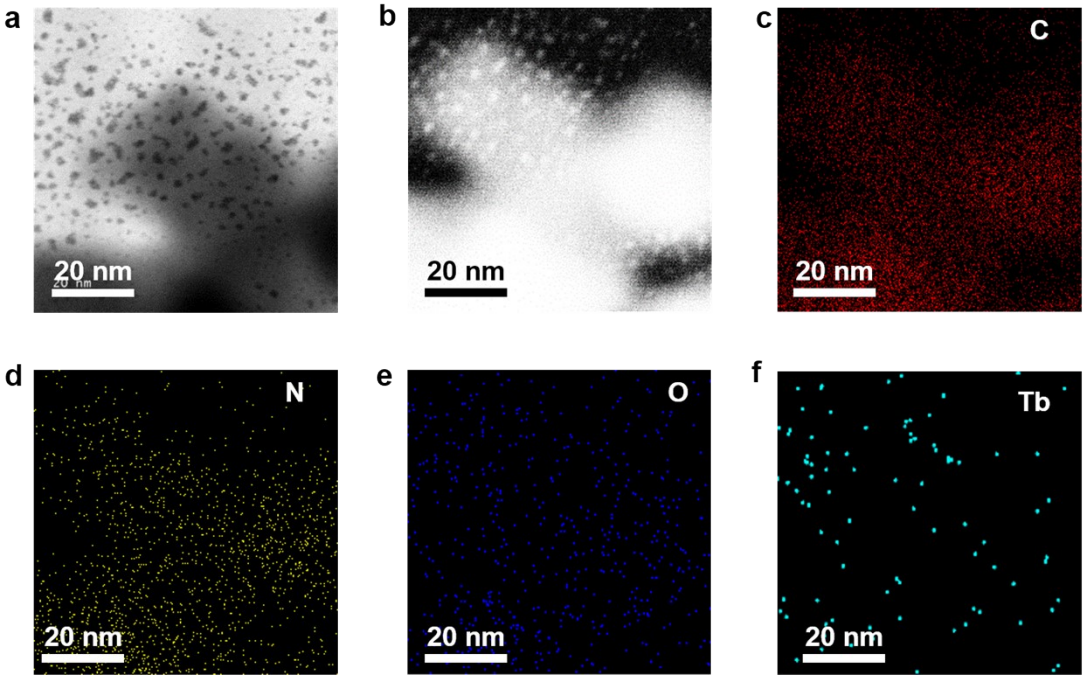

Figure S11. (a) TEM image of TbCs-COF1. (b-f) EDS mapping of TbCs-COF1.

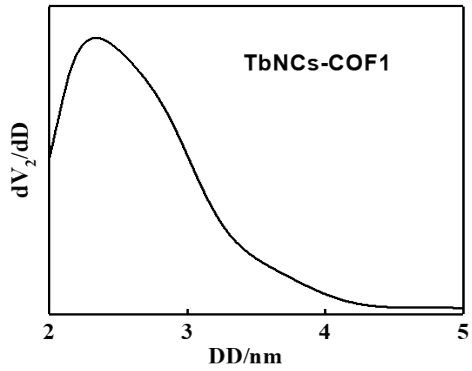

Figure S12. Pore size distribution of TbCs-COF1.

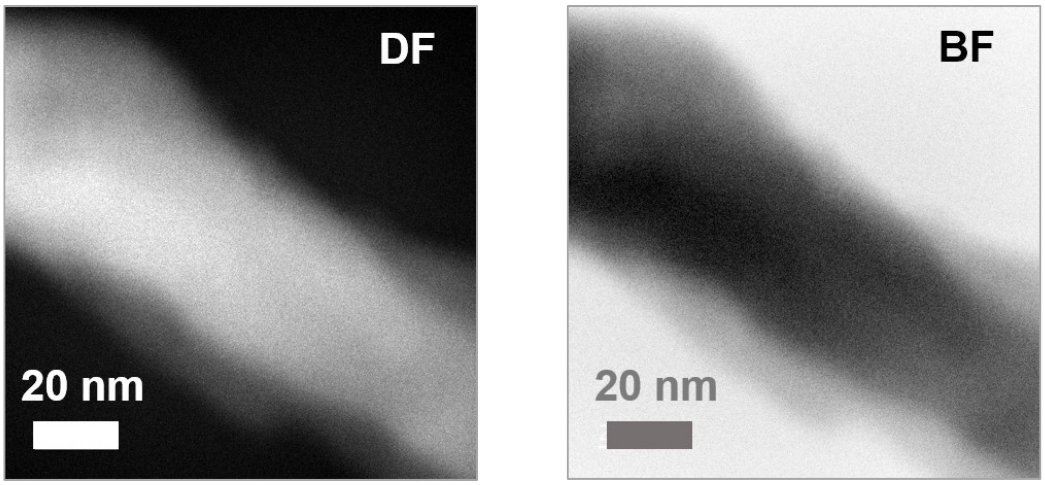

Figure S13. HAADF images of COF1-Heck. DF represents dark field. BF represents bright field.

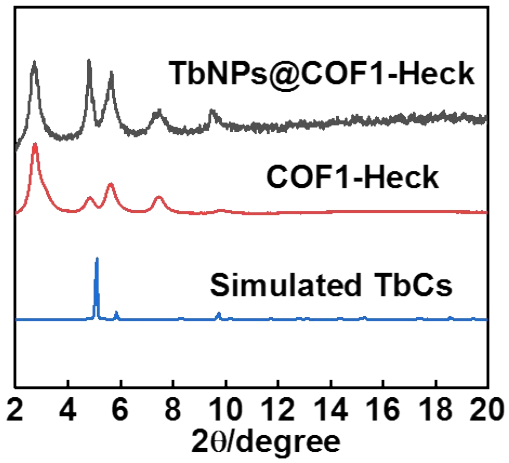

Figure S14. XRD patterns of COF1-Heck and TbNPs@COF1-Heck, respectively.

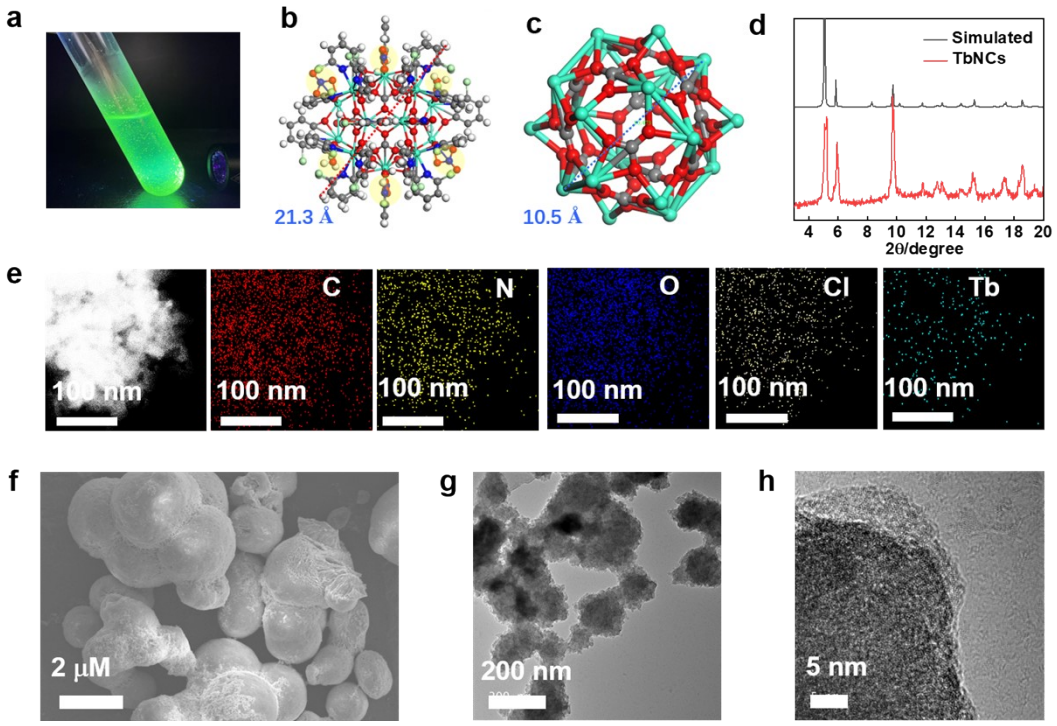

Figure S15. (a) The formed crystal of the pure TbCs. (b) Molecular structure of the pure TbCs. (c) Molecular structure of the metal core of the pure TbCs with no CHP on the surface. (d) Simulated and experimental PXRD patterns of the pure TbCs. Inset: photos of the pure TbCs under sunlight and UV light. (e) EDS mapping of the pure TbCs. (f) SEM image of the pure TbCs. (g and h) TEM images of the pure TbCs.

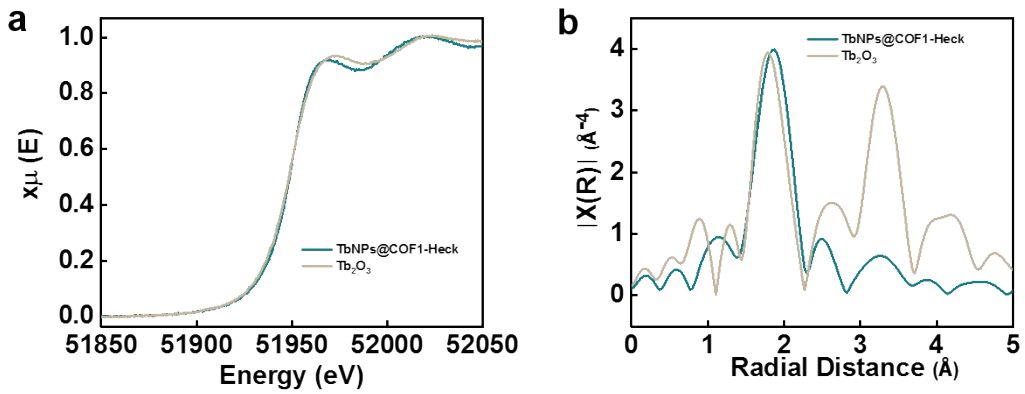

Figure S16. (a) The comparison of Tb K-edge XANES spectra. (b) The comparison of Tb K-edge EXAFS, shown in k^3 weighted *R*-space.

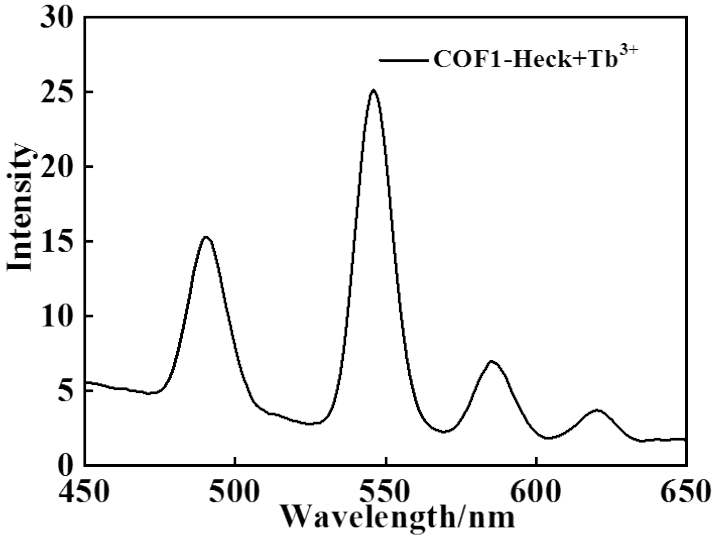

Figure S17. The confirmation of the sensitization effect of COF1-Heck to Tb^{3+} by directly adding $Tb(NO_3)_3 \cdot 6H_2O$ to the COF1-Heck suspension.

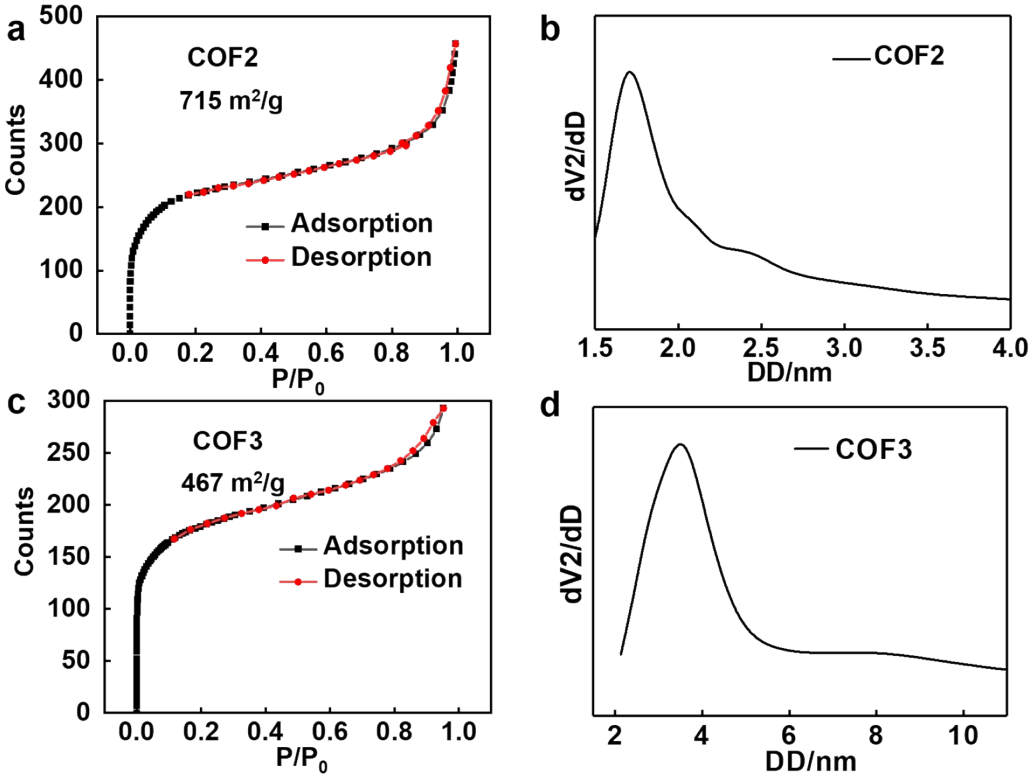

Figure S18. . (a) N_2 isothermal adsorption-desorption curve and (b) pore size distribution of COF2. (c) N_2 isothermal adsorption-desorption curve and (d) pore size distribution of COF3.

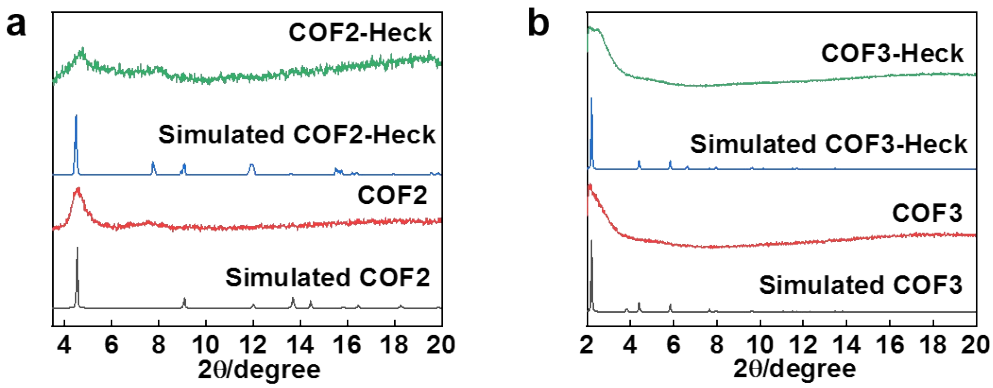

Figure S19. (a) Experimental powder and simulated XRD patterns of COF2 and COF2-Heck, respectively. (b) Experimental powder and simulated XRD patterns of COF3 and COF3-Heck, respectively.

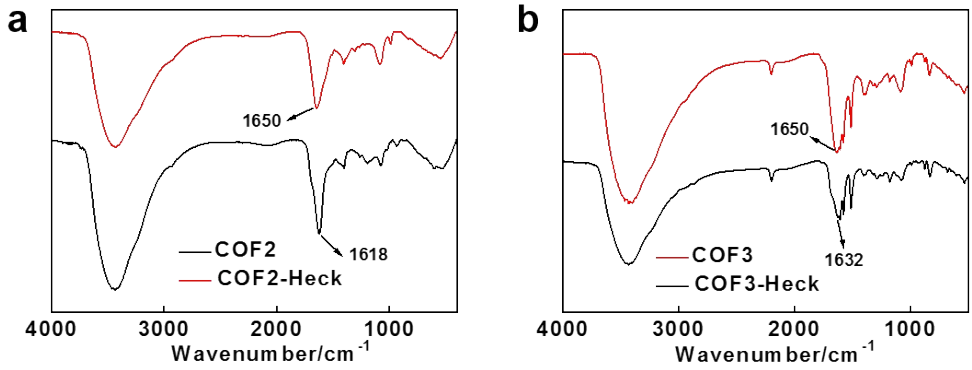

Figure S20. (a) FTIR spectra of COF2 and COF2-Heck, respectively. (b) FTIR spectra of COF3 and COF3-Heck, respectively.

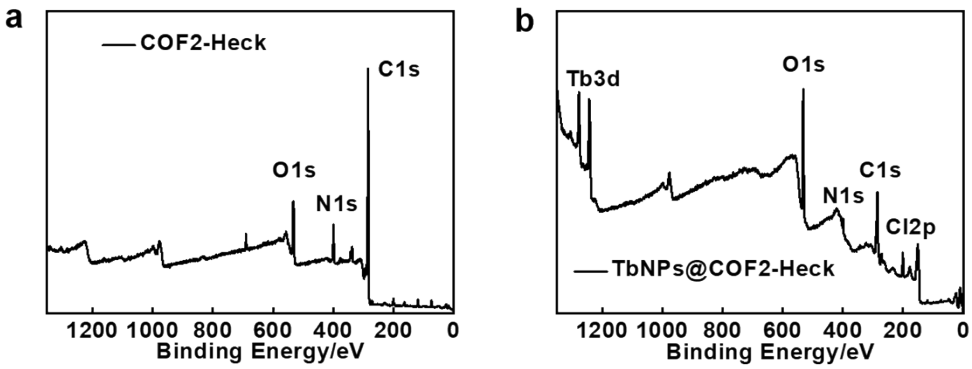

Figure S21. (a) XPS spectrum of COF2-Heck. (b) XPS spectrum of TbNPs@COF2-Heck.

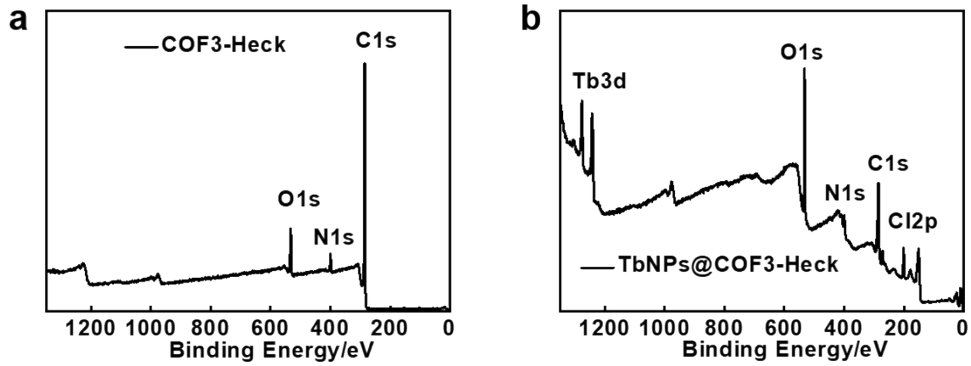

Figure S22. (a) XPS spectrum of COF3-Heck. (b) XPS spectrum of TbNPs@COF3-Heck.

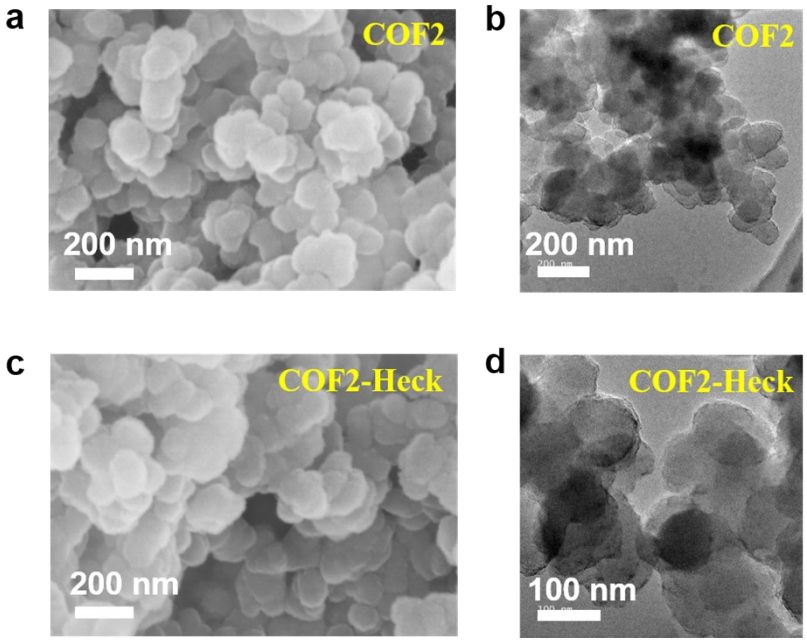

Figure S23. (a) SEM and (b) TEM images of COF2. (c) SEM and (d) TEM images of COF2-Heck.

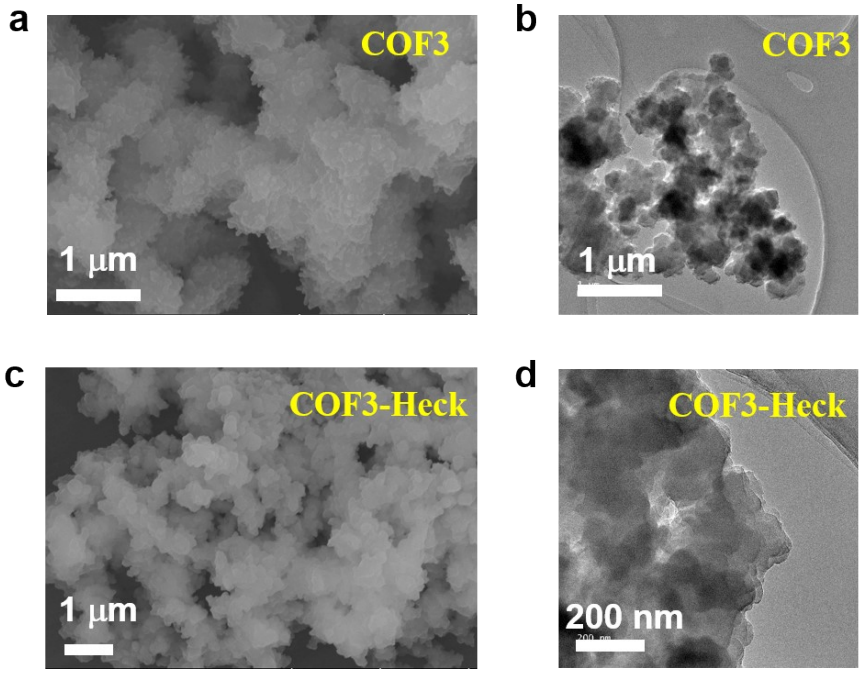

Figure S24. (a) SEM and (b) TEM images of COF3. (c) SEM and (d) TEM images of COF3-Heck.

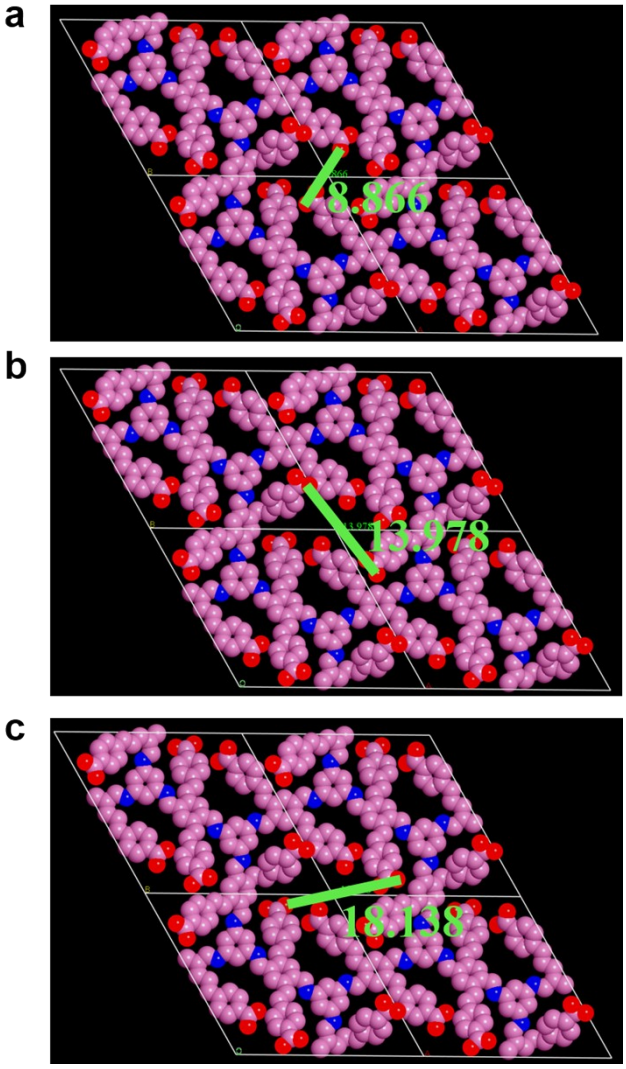

Figure S25. The distances of two opposing carboxyl groups in COF2-Heck, which were stimulated in Materials Studio.

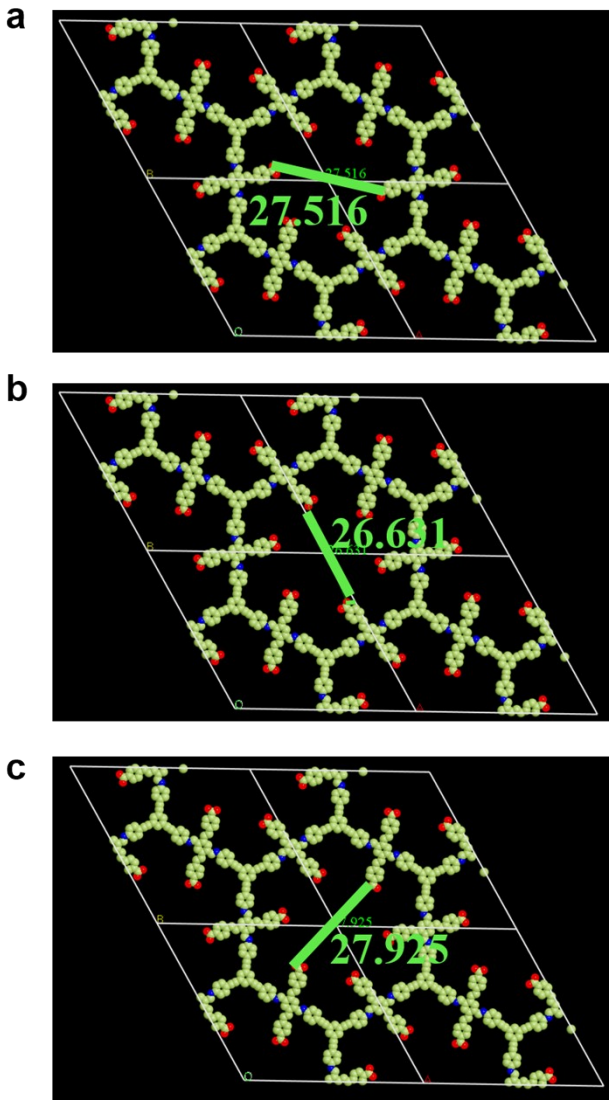

Figure S26. The distances of two opposing carboxyl groups in COF3-Heck, which were stimulated in Materials Studio.

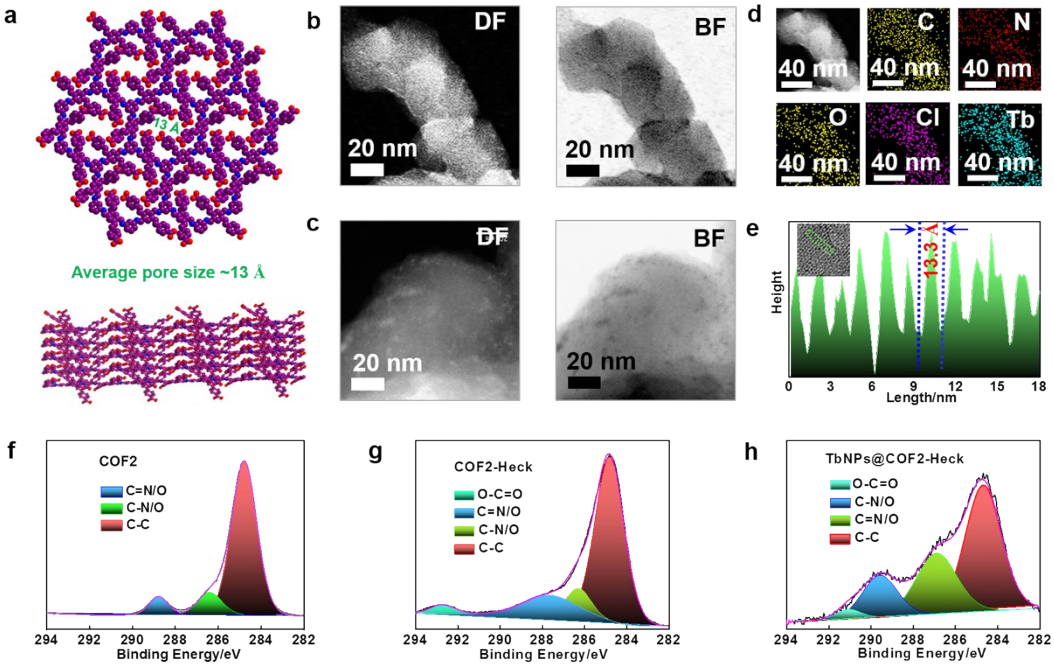

Figure S27. (a) AA stacking mode of COF2-Heck with the C atoms in purple, the N atoms in blue, and the O atoms in red (H omitted for clarity). The average carboylated nanochannel diameter was simulated to be about 13 Å. (b) HAADF images of TbNPs@COF2-Heck. (c) HAADF images of COF2-Heck. (d) EDS mapping of the C, N, O, Cl and Tb elements in TbNPs@COF2-Heck. (e) Size distribution of the TbNPs in COF2-Heck. Inset: size distribution of the TbNPs deriving from the highlight region of TbNPs@COF2-Heck. (f) Refined C1s spectrum of COF2. (g) Refined C1s spectrum of COF2-Heck. (h) Refined C1s spectrum of TbNPs@COF2-Heck.

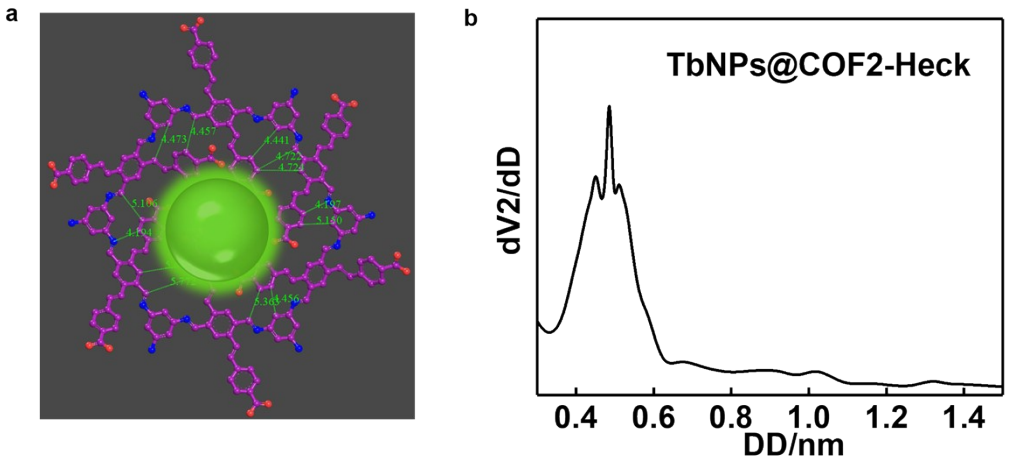

Figure S28. (a) Simulated minimum width of the secondary pores of TbNPs@COF2-Heck. (b) Pore size distribution of TbNPs@COF2-Heck.

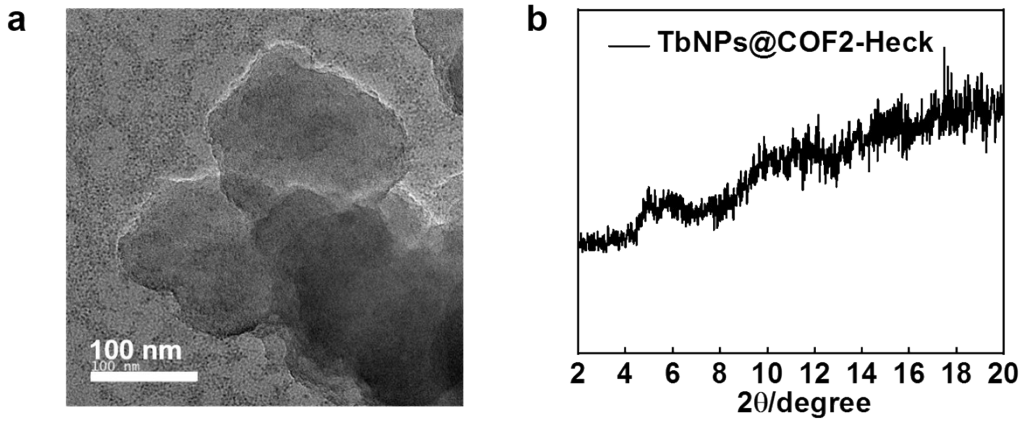

Figure S29. (a) TEM image of COF2-TbCs. (b) XRD patterns of TbNPs@COF2-Heck.

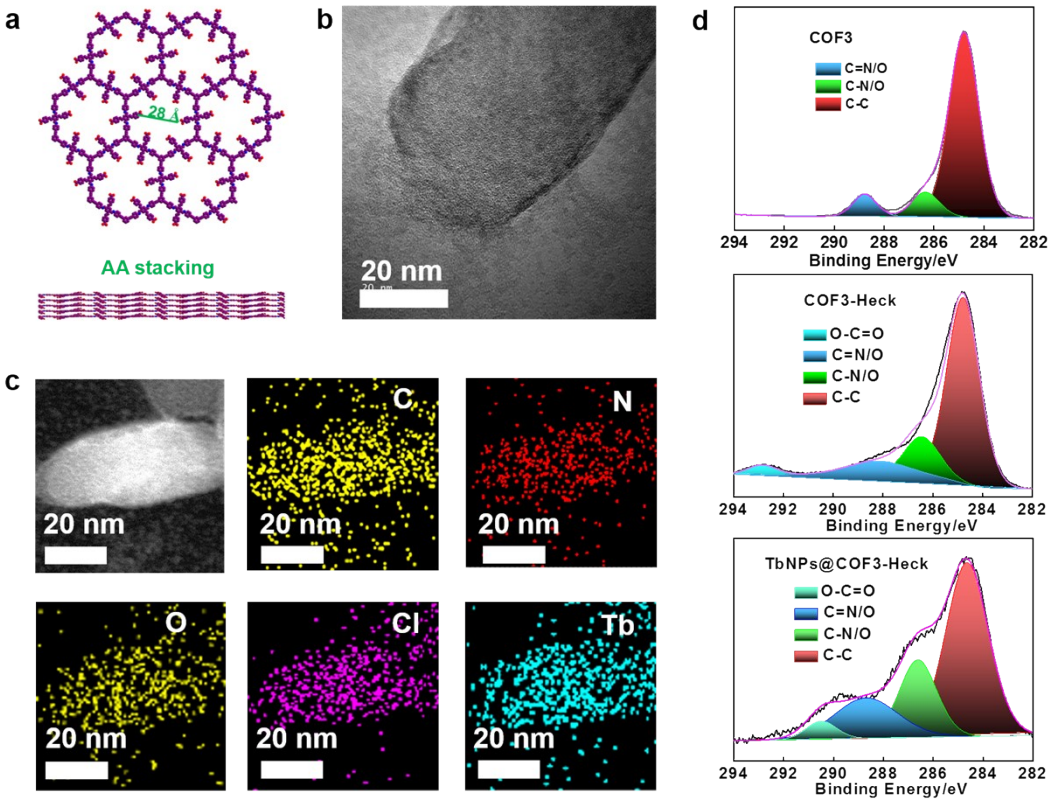

Figure S30. (a) AA stacking mode of COF3-Heck with the C atoms in purple, the N atoms in blue, and the O atoms in red (H omitted for clarity). The carboylated cavity size was simulated to be about 28 Å. (b) TEM image of TbNPs@COF3-Heck. (c) EDS mapping of the C, N, O, Cl and Tb elements in TbNPs@COF3-Heck. (d) Refined C1s spectra of COF3, COF3-Heck and TbNPs@COF3-Heck, respectively.

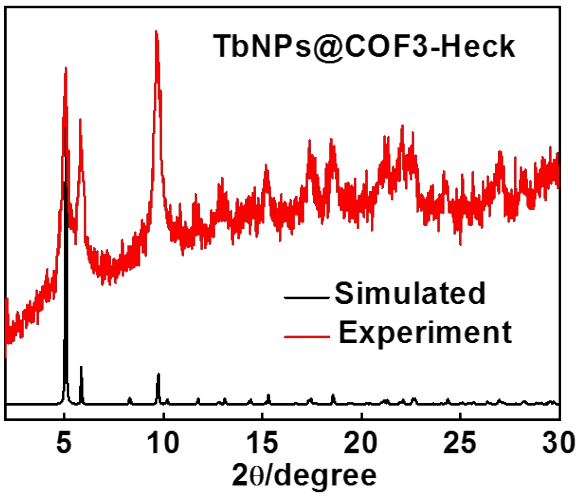

Figure S31. Experimental XRD patterns of TbNPs@COF3-Heck and simulated XRD patterns of the pure TbCs.

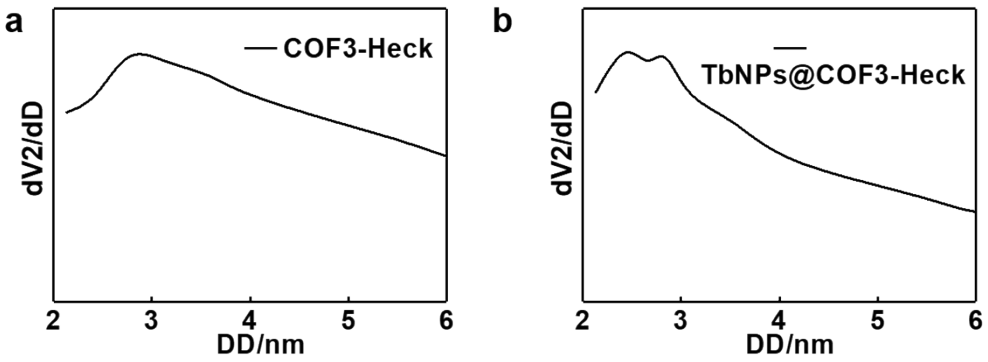

Figure S32. (a) Pore size distribution of COF3-Heck. The wide pore size distribution of COF3-Heck indicated that the Heck reaction influenced the regular structure of the COF3. (b) Pore size distribution of TbNPs@COF3-Heck.

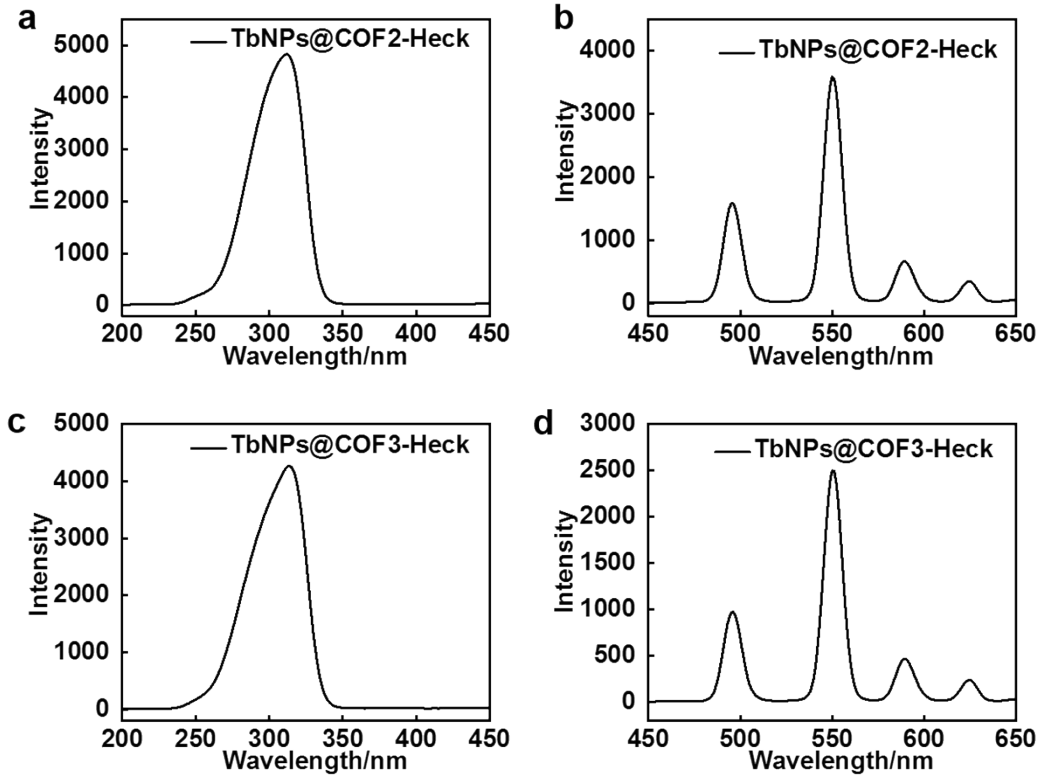

Figure S33. (a) Excitation and (b) emission spectra of TbNPs@COF2-Heck, respectively. (c) Excitation and (d) emission spectra of TbNPs@COF3-Heck, respectively.

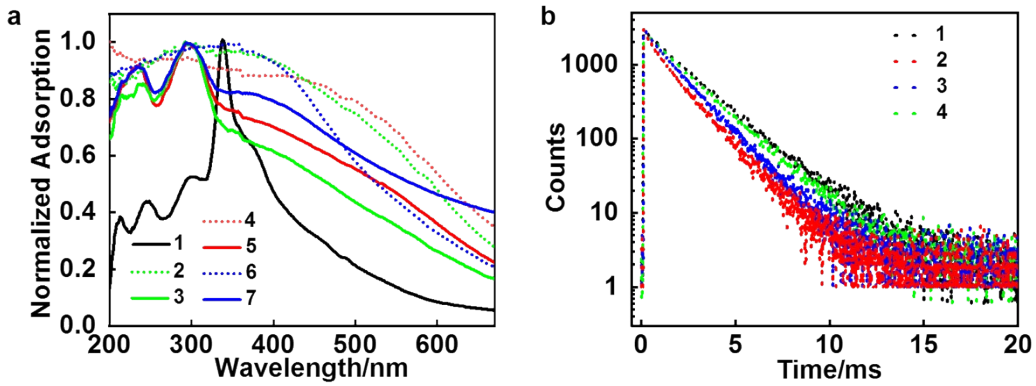

Figure S34. (a) UV-vis adsorption spectra of the pure TbCs (curve 1), COF1-Heck (curve 2), TbNPs@COF1-Heck (curve 3), COF2-Heck (curve 4), TbNPs@COF2-Heck (curve 5), COF3-Heck (curve 6) and TbNPs@COF3-Heck (curve 7), respectively. (b) Fluorescent lifetimes decay curves of the pure TbCs (curve 1), TbNPs@COF1-Heck (curve 2), TbNPs@COF2-Heck (curve 3) and TbNPs@COF3-Heck (curve 4), respectively.

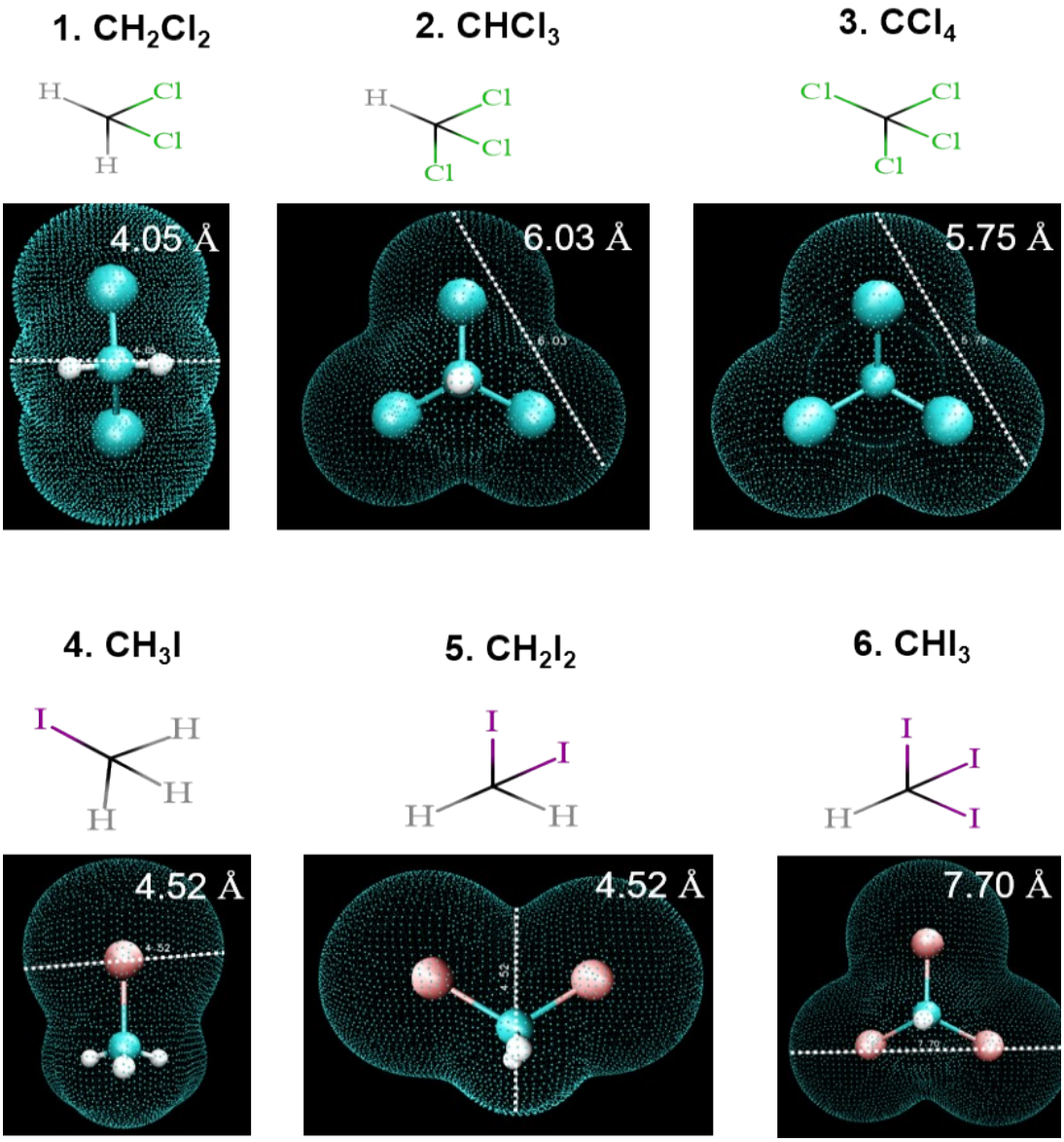

Figure S35. The minimum limit sizes of CH_2Cl_2, $CHCl_3$, CCl_4, CH_3I, CH_2I_2 and CHI_3 calculating from Gaussian based on the dynamics at zero Jones potential.

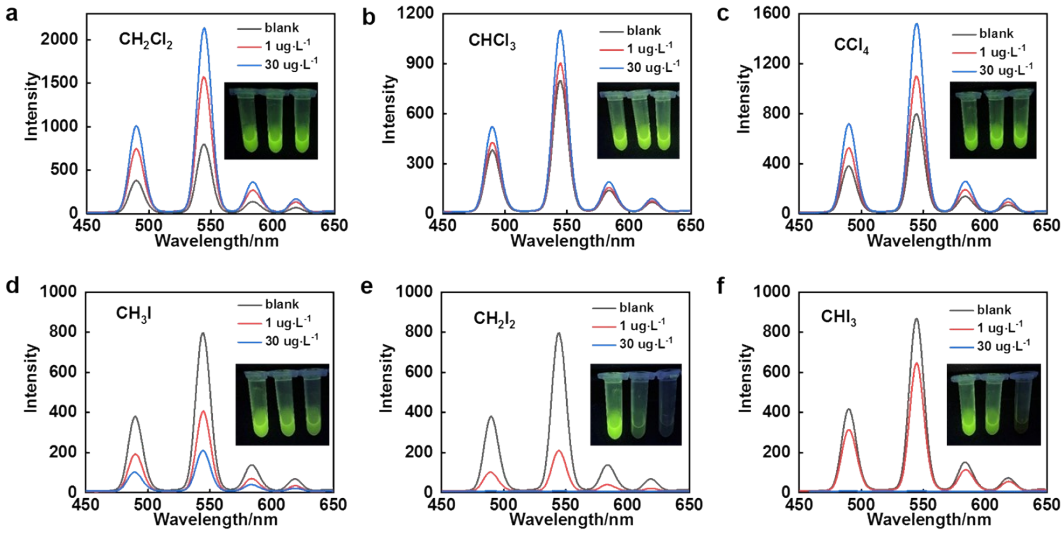

Figure S36. Fluorescent spectra of TbNPs@COF2-Heck treated with different contents of (a) CH_2Cl_2, (b) $CHCl_3$, (c) CCl_4, (d) CH_3I, (e) CH_2I_2, and (f) CHI_3 in methanol, respectively.

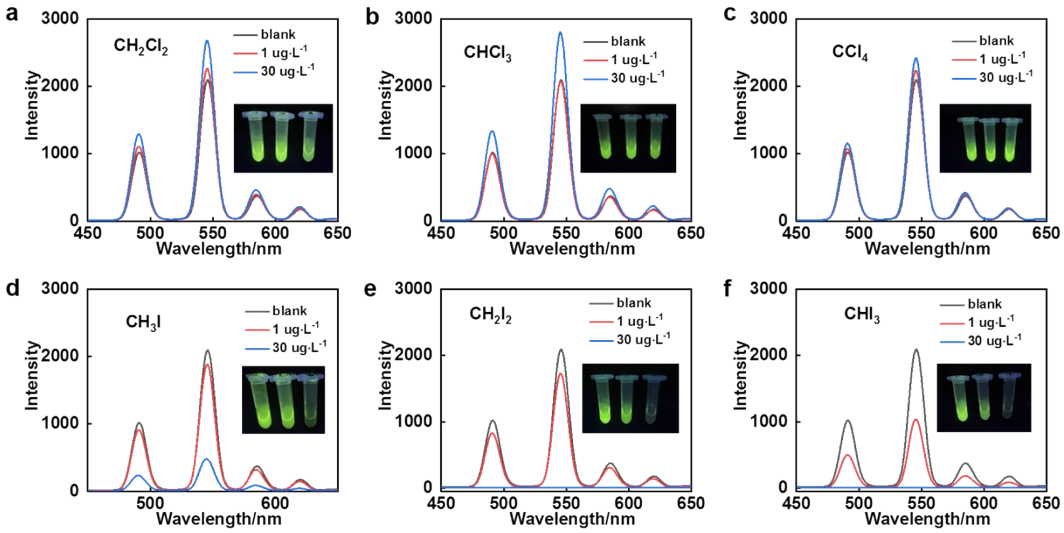

Figure S37. Fluorescent spectra of the pure TbCs treated with different contents of (a) CH_2Cl_2, (b) $CHCl_3$, (c) CCl_4, (d) CH_3I, (e) CH_2I_2, and (f) CHI_3 in methanol, respectively.

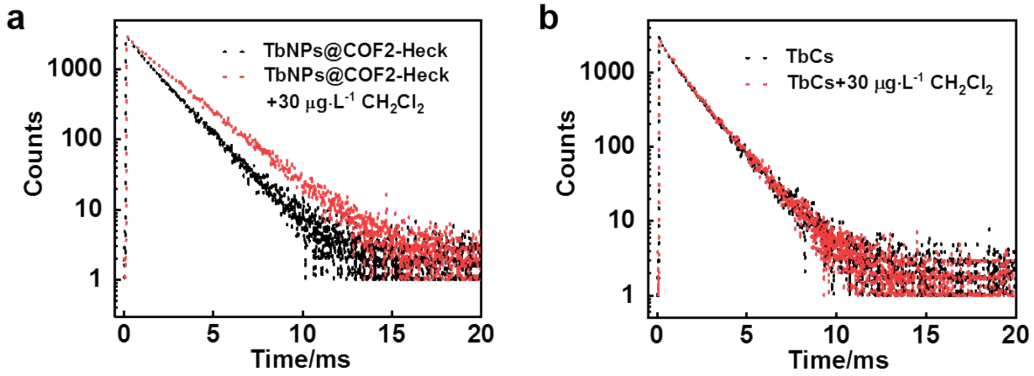

Figure S38. (a) Fluorescent lifetimes of TbNPs@COF2-Heck before and after being treated with 30 μg·L^{-1} CH_2Cl_2, respectively. (b) Fluorescent lifetime of the pureTbCs before and after being treated with 30 μg·L^{-1} CH_2Cl_2, respectively.

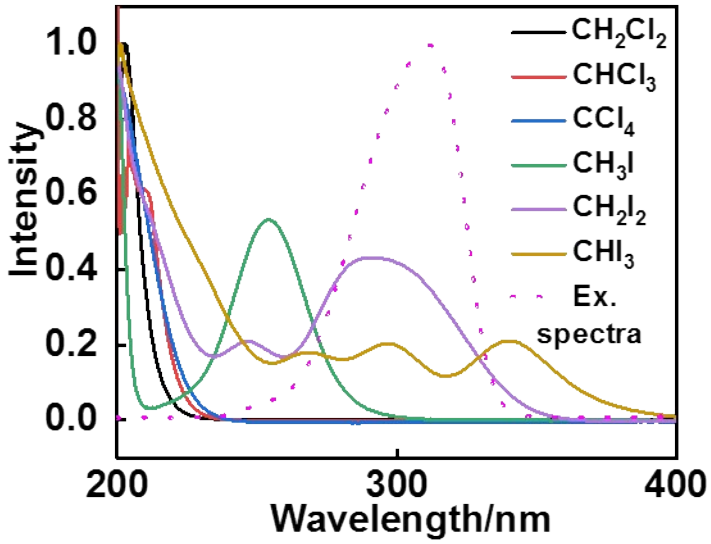

Figure S39. UV-vis adsorption spectra of CH_2Cl_2, $CHCl_3$, CCl_4, CH_3I, CH_2I_2 and CHI_3, respectively, and the excitation spectra of TbNPs@COF2-Heck.

Table S1. Single crystal analysis and EXAFS fitting parameters at the Tb K-edge for TbCs and TbNPs@COF1-Heck, respectively. (S_0^2=1.0).

Method	Sample	Shell	*CN*[a]	*R*(Å)[b]	σ^2(Å^2)[c]	ΔE_0(eV)[d]	*R* factor
Single crystal analysis	TbCs	Tb-O and Tb-N	6	2.3±0.1	-	-	-
EXAFS analysis	TbNPs@COF1-Heck	Tb-O and Tb-N	5.9 ±0.5	2.37±0.01	0.0084 ±0.0014	5.2	0.0083

[a]*CN*, nominal coordination number; [b]*R*, distance between absorber and backscatter atoms; [c]σ^2, Debye-Waller factor to account for both thermal and structural disorders; [d]ΔE_0, inner potential correction; *R* factor indicates the goodness of the fit. $S0^2$ was fixed to 1.0. Fitting range: 2.0 ≤ *k* (/Å) ≤ 10.5 and 1.0 ≤ *R* (Å) ≤ 2.5 (Tb1); 2.0 ≤ *k* (/Å) ≤ 10.5 and 1.0 ≤ *R* (Å) ≤ 2.5 (Tb2 and Tb3). A reasonable range of EXAFS fitting parameters: 0.700 < S_0^2 < 1.000; *CN* > 0; σ^2 > 0 Å^2; ΔE_0 < 10 eV; *R* factor < 0.02.

Table S2. The fluorescent lifetimes of the pure TbCs and TbNPs@COFs-Heck.

Materials	Wavelength	A_1	τ_1 (ms)	Percent (%)	A_2	τ_2 (ms)	Percent (%)	R	τ_{avg} (ms)
TbCs	545 nm	0.96	1.86	100	-	-	-	0.999	1.86
TbCs+CH_2Cl_2	545 nm	0.97	1.89	100	-	-	-	0.997	1.89
TbNPs@COF1-Heck	545 nm	0.24	0.32	6.3	0.75	1.43	93.7	0.999	1.36
TbNPs@COF2-Heck	545 nm	0.17	0.60	7.1	0.83	1.61	92.9	0.999	1.54
TbNPs@COF2-Heck+ CH_2Cl_2	545 nm	0.13	0.63	4.2	0.86	2.07	95.8	0.999	2.01
TbNPs@COF3-Heck	545 nm	0.10	0.47	2.9	0.89	1.83	97.1	0.999	1.79

Comments: The fluorescent lifetimes were fitted with the equation of

$$\tau_{avg} = \frac{A_1\tau_1^2 + A_2\tau_2^2}{A_1\tau_1 + A_2\tau_2}.$$

It could be clearly seen that the decay curve of the pure TbCs was single-exponential, while those of TbNPs@COF1-Heck, TbNPs@COF2-Heck and TbNPs@COF3-Heck were double-exponential. This discrepancy should be attributed to the fact that the COFs-Heck were capable of transferring energy to Tb^{3+} and functioned as auxiliary ligands besides CHP. It was observed that TbNPs@COF3-Heck possessed the least short-lived component (τ_1), and the lifetime of its long-lived component (τ_2) was the closest to the pure TbCs. This result also demonstrated that TbNPs were dominantly aggregated on the outer surfaces of COF3-Heck other than embedding in the pores.

Table S3. Comparison with various fluorescent sensing strategies for detection of UO_2^{2+}.

Methods	Materials	LOD(nM)	References
Fluorescence	Ln-MOFs-1	2.78	5
Fluorescence	Ln-MOFs-2	30.9	6
Fluorescence	Ln-MOFs-3	3.3	7
Fluorescence	Ln-MOFs-4	0.75	8
Fluorescence	Fluorescent organic dye	0.74	9
Fluorescence	Lanthanide coordination polymer	1420	10
Fluorescence	COFs	6.7	11
Fluorescence	CQDs	4	12
Fluorescence	LnCs	35	This work
Fluorescence	LnCs composite	0.38	This work

References

1. D. Galico, A. Kitos, J. Ovens, F. Sigoli, M. Murugesu, *Angew. Chem. Int. Ed.,* 2021**, 60**, 6130-6136.

2. D. Gálico, M. Murugesu, *ACS App. Mater. Interfaces,* 2021**, 13**, 47052-47060.

3. Y. Zhou, X. Zheng, J. Cai, Z. Hong, Z. Yan, X. Kong, Y. Ren, L. Long, L. Zheng, *Inor. Chem.,* 2017**, *56***, 2037-2041.

4. B. Ravel, M. Newville, *J. Synchro. Rad.,* 2005**, 12**, 537-541.

5. M. Lei, Y. Jia, W. Zhang, J. Xie, Z. Xu, Y. Wang, W. Du, W. Liu, *ACS App. Mater. Interfaces,* 2021, **13**, 51086-51094.

6. J. Ye, R. Bogale, Y. Shi, Y. Chen, X. Liu, S. Zhang, Y. Yang, J. Zhao, G. Ning, *Chem. Eur. J.,* 2017, **23**, 7657-7662.

7. W. Liu, X. Dai, Z. Bai, Y. Wang, Z. Yang, L. Zhang, L. Xu, L. Chen, Y. Li, D. Gui, J. Diwu, J. Wang, R. Zhou, Z. Chai, S. Wang, *Environ. Sci. Technol.,* 2017, **51**, 3911-3921.

8. Y.-J. Tong, L.-D. Yu, Y. Huang, Q. Fu, N. Li, S. Peng, S. Ouyang, Y.-X. Ye, J. Xu, F. Zhu, J. Pawliszyn, G. Ouyang, *Anal. Chem.* 2021, **93**, 9226-9234.

9. X. Chen, L. He, Y. Wang, B. Liu, Y. Tang, *Anal. Chim. Acta,* 2014, **847**, 55-60.

10. M. Wang, Z. Liu, X. Zhou, H. Xiao, Y. You, W. Huang, *Inor. Chem.,* 2020**, 59**, 18027-18034.

11. W.-R. Cui, C.-R. Zhang, W. Jiang, F.-F. Li, R.-P. Liang, J. Liu , J.-D. Qiu, *Nat. Commun.* 2020, **11**, 436.

12. X. Chen, Q. Mei, L. Yu, H. Ge, J. Yue, K. Zhang, T. Hayat, A. Alsaedi, S. Wang, *ACS App. Mater. Intererfaces,* 2018, **10**, 42225-42232.